Experimental characterization of thrust production mechanisms in a magnetic nozzle ECR thruster

Federico Boni, Victor Désangles, Julien Jarrige

Experimental characterization of thrust production mechanisms in a magnetic nozzle ECR thruster

IEPC-2022-528

Presented at the 37th International Electric Propulsion Conference
Massachusetts Institute of Technology, Cambridge, MA USA
June 19-23, 2022

Federico Boni[1], Victor Désangles[2]
ONERA, Université Paris-Saclay, F-91123Palaiseau, France

Julien Jarrige[3]
ONERA, Université Toulouse, F-31055 Toulouse, France

Direct thrust measurements have been performed on a low-power (30 W) ECR plasma thruster operated with xenon. The total thrust, the force exerted on the walls of the source (thermal thrust), and the force exerted on the permanent magnet (magnetic thrust) have been measured separately for various operating conditions (power and flowrate). The results are compared for two magnetic field topologies (with a different magnetic field gradient). The magnetic thrust dominates thermal thrust for most of the operating conditions, and its contribution to total thrust can be as high as 80%. A saturation of magnetic thrust with increasing power has been observed, and correlated with a decrease of thrust efficiency.

I. Introduction

Electrodeless magnetic nozzle thrusters have received a great attention these last few years for their ability to produce thrust without the need of an external cathode neutralizer, the possibility to work with various propellants (including reactive gases like water or oxygen), and the theoretically lower wall erosion in the plasma source. The principle of magnetic nozzle (MN) is the conversion of electrons gyrokinetic energy into ions axial momentum, which generates thrust. Because of the high complexity of the MN physics, there is still a low understanding of the parameters (geometry, magnetic field topology) that could help improving MN thrusters performances.

Recently, several theoretical works have investigated the thrust production mechanisms in MN thrusters [1, 2]. Using a fluid description for the plasma, these works have shown that the thrust has two main components:

- the thermal thrust T_S , which is due to the electron pressure and is exerted on the backwall of the thruster;
- the magnetic thrust T_B, which is due to the force exerted by electrons on the externally applied magnetic field. $T_B$is a volumic force (exterted on the whole plasma volume, including the plume) that is due to diamagnetic effects.

Experimental measurements of electron pressure, thrust components T_B and T_S on a helicon thruster have been compared with a 2D model [3]. The magnetic thrust is seen to increase with the magnetic field strength, and T_B contribution to total thrust can be higher than 50%.

The ECR (electron cyclotron resonance) plasma thruster is an electrodeless MN thruster that uses microwave power to ionize the gas and heat the electrons. ECR thrusters are characterized by a high magnetic field strength in the resonance region (~ 1000 G), and a different electron heating process than in helicon thrusters: the energy is initially injected mainly in the gyrokinetic mode. These features are favorable for the production of thrust with a good efficiency.

[1] PhD student, Physics Instrumentation and Space Department, federico.boni@onera.fr
[2] Research Scientist, Physics Instrumentation and Space Department, victor.desangles@onera.fr
[3] Research Scientist, Physics Instrumentation and Space Department, julien.jarrige@onera.fr

In this work, an experimental investigation of the thrust production mechanisms is carried out on a low power ECR plasma thruster operated with xenon. Direct measurements of the total thrust, of the force exerted on the plasma source, and of the force exerted on the permanent magnet have been performed with a thrust balance. Two different magnetic field topologies (with a different divergence) have been studied. The contribution of T_B and T_S to total thrust and the thruster performances are investigated as a function of the operating parameters (mass flow rate and microwave power).

II. Apparatus

A. ECR thruster

The thruster investigated is the electron cyclotron resonance (ECR) plasma thruster that has been developed at ONERA since 2010. The originality of this thruster is its coaxial geometry that allows to have a compact geometry (27 mm diameter) while being operated with microwave at frequencies of 2.45 GHz. The ECR thruster version that is characterized in this work is the 30 W model, which is shown in Figure 1. The plasma source is 20 mm long and consists of an inner rod (2.3 mm in diameter) and an outer cylinder (27.5 mm in diameter). The end of the source is closed with a boron nitride (BN) disk (transparent to microwaves) that prevents the plasma from eroding the coaxial microwave transmission line. The propellant gas is injected in the source with two alumina tubes (1 mm diameter) through the BN backplate. In this study, only xenon has been used for the experiments.

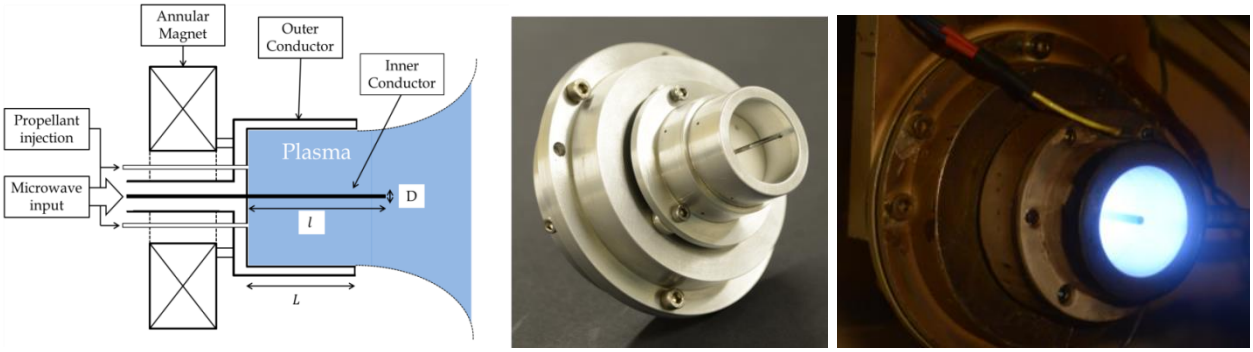

Figure 1. Schematics of ECR thruster (left), and views of 30 W ECR model (right: operated with xenon).

The magnetic field is provided by an annular permanent magnet located at the back of the plasma source. Two different magnetic field configurations (called BM and SM) have been used for this study. The topologies of the magnetic field lines in the source and in the magnetic nozzle are shown in Figure 2. The position of the resonance region (around 875 G) with respect to the backplate is similar for both configurations, but the BM configuration displays a more divergent magnetic field, hence a steeper magnetic field axial gradient: $\frac{\partial B}{\partial z}$ in the source is about 1.5 times higher for configuration BM than for configuration SM.

The thruster is powered by a Microwave Amp Ltd amplifier driven by a VAUNIX LMS-402D signal generator. The forward and reflected power (to the thruster) are measured with two LB478A (Ladybug technologies) calibrated power sensors using directional couplers. The transmission line is characterized (in terms of power losses) with a vector network analyzer prior to the experiments so that the deposited power absorbed by the plasma can be computed.

The thruster body and the inner rod are electrically floating, so that the plasma plume remains current free.

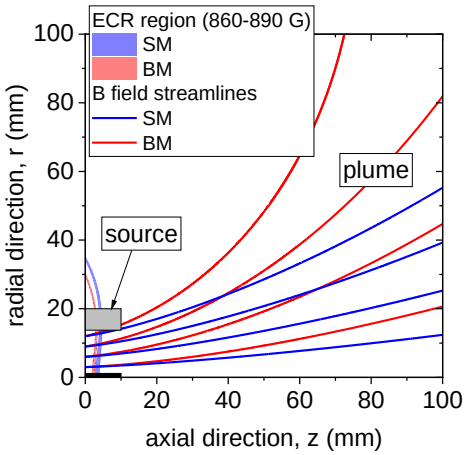

Figure 2. Topology of the magnetic field lines for the magnetic configurations SM and BM.

B. Thrust balance

The total thrust and the magnetic and thermal components of thrust are measured using ONERA milli-newton thrust balance. This balance, which is described in details in [4], is a vertical pendulum of compound type with a quasi-frictionless pivot (see Figure 3). The thruster is mounted at the end of the pendulum arm, on which it applies a horizontal force. In the free pendulum mode, the arm then moves from its initial position to a new, tilted equilibrium position, where the torques exerted by the thrust and by the weigth of the pendulum arm cancel each other. The angle of the pendulum is then a linear measure of the thrust, given that the angle is usually very small (<< 1 degree). Two displacement sensors are placed on the pendulum arm: one is an accelerometer (Honeywell QA 700) for which the axis measures the projection of gravity; the other is a capacitive sensor (Focale MC 900) that measures the linear displacement of the arm.

A coil actuator is placed at the bottom of the pendulum. It consists of a permanent magnet fixed on the arm near a planar coil placed on the vacuum tank. When making a current flow through the coil, a force is applied on the arm. Because of the frictionless movement of the coil, and provided that the movement is very small, this force is proportional to the current.

Two measurement modes can be used:

- Open loop: as described above, where the pendulum is free to move ;
- Closed loop: a feedback loop uses the coil actuator to maintain the pendulum at its initial equilibrium position. This mode has one clear advantage: the movement of the pendulum becomes second order. This is important if the movement is perturbed by non-linear flexure phenomena (like plastic deformation of gas tubes and cables), because these effects will be dramatically reduced.

All thrust measurements performed during this campaign were done in closed loop mode. The current through flowing though the coil actuator is controlled with a Proportional-Integrator-Derivative (PID) system. The process variable is the signal of the capacitive sensor, which is fed to the PID controller (SRS SIM960). When the thruster applied a force on the pendulum, the PID output signal is modified, and the resulting magnetic field interacts with the permanent magnet to produce a force. The output voltage from the PID controller is directly proportional to the force applied by the thruster, provided that the error is small enough. The thrust can then be measured from the PID signal, knowing the calibration factor.

One of the advantages of a pendulum balance is that it allows for an absolute and precise thrust calibration. The principle is to deposit masses on a small horizontal arm attached to the pendulum. The weights of the masses are calibrated very precisely with a Mettler Toledo balance precise to 0.01 mg. The masses are placed on a vertical translation stage, and are deposited sequentially on the calibration arm, thus imposing calibrated torques on the balance.

In the past few years, ONERA milli-newton balance has been successfully used for direct thrust measurements of ECR thruster [4] as well as other low power electric propulsion technologies: gridded ion engine [5], helicon [6], HET [7].

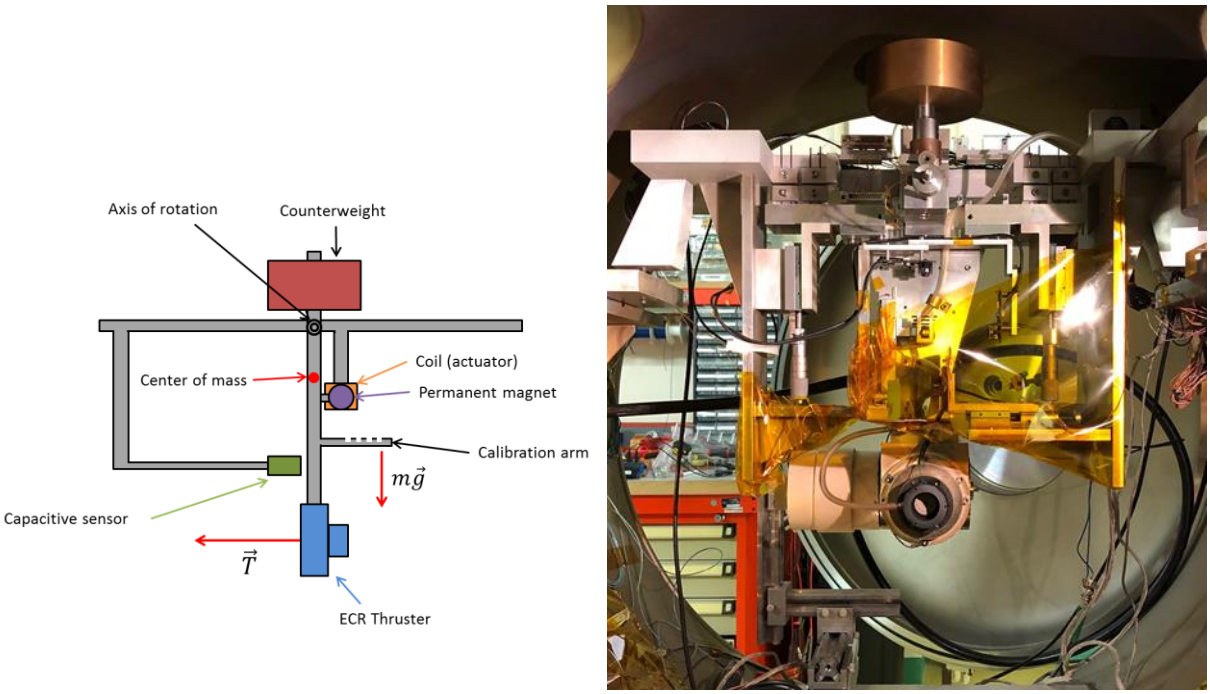

Figure 3. Schematics and view of the thrust balance

C. Facility and setup

The experimental characterization of thrust production mechanisms has been performed in B09 vacuum chamber (0.8 m in diameter, 2 m long) at ONERA center of Palaiseau. The secondary pumping consists of three turbo-molecular pumps (Pfeiffer Hi-Pace 2300) and a cryogenic pump (Sumitomo CH-110 cryo-cooler), yielding a total pumping speed of 13 000 L/s for xenon, with a base pressure around $2\text{x}10^{-7}$ mbar. In the conditions of this study (xenon flowrate between 0.7 sccm and 2 sccm), the background pressure is in the range $1\text{-}2.6\text{x}10^{-6}$ mbar.

The propellant mass flowrate injected in the thruster is controlled with a Bronkhorst El-Flow controller with a full scale of 4 sccm calibrated for xenon.

For this test campaign, the thrust balance has been adapted to B09 vacuum chamber, whose diameter is smaller than the chamber used for previous tests (1 m) [4]. In order to maintain the position of the thruster at the center of the vessel, the pendulum arm was shortened, which has resulted in a more compact setup with the thruster being placed closer to the balance structure.

Three different setups are used:

- For total thrust measurements, the whole thruster assembly (coaxial cavity + permanent magnets) is mounted on the pendulum arm.
- For the measurement of the thermal thrust T_S (produced by thermal expansion of electrons), the coaxial cavity (with the gas injection and the microwave transmission line) is mounted on the pendulum arm, while the permanent magnets is fixed to the vessel.
- For the measurement of the magnetic thrust T_B, the permanent magnet is mounted on the arm, while the coaxial cavity is fixed to the vessel.

It should be noted that, for the second setup, the measured thrust actually corresponds to the total force exerted on the walls of the source, i.e. the sum of the axial force on the backplate (due to electron pressure) and the axial momentum on the cylindrical walls (due to ions). Measurements on a helicon thruster [3] have shown that the force due to ions on the radial walls becomes negligible when the magnetic field in the source is high enough (above ~100 Gauss). Considering the high magnetic field in the coaxial source of the ECR thruster (between 500 and 1000 Gauss) and the low observed axial velocity of ions in this region [8], the force exerted on the source walls can then be considered as due to the electron pressure contribution only.

For the separate thrust measurements, special attention was paid to have the shell of the permanent magnet and the source outer cylinder electrically floating. Furthermore, they were electrically connected (with flexible wires) in order to be consistent with the electrical configuration of total thrust measurements. The absolute position of the resonance region with respect to the source backwall was accurately set for each mounting.

III. Results

The total thrust, the magnetic and thermal components have been measured as a function of microwave power (between 10 and 60 W) for different xenon mass flowrates (0.7 sccm to 2 sccm). The results obtained with configuration SM and configuration BM are shown in Figure 4 and Figure 5, respectively. The error bars correspond to the 1-sigma uncertainty calculated with the error budget detailed in [4]. In the range of thrust levels that are measured in this work, the budget error is dominated by the uncertainty on the calibration coefficient. The sum of magnetic and thermal components is also computed and is used for verification of the thruster repeatability when changing the balance and the thruster setup. It can be seen that total thrust and the sum of T_B and T_S are in good agreement for all operating conditions, so the respective contributions of the two thrust components can be considered reliable for further analyses.

Overall, the total thrust increases with power for all xenon flowrates and for the two magnetic configurations. The thrust increase rate tends to saturate above a power of 40 W, especially for the lowest flowrates. This is mainly due to the behavior of magnetic thrust. On one hand, for all flowrates and for the two magnetic configurations, the thermal thrust T_S (red circles) is seen to increase steadily with microwave power. On the other hand, the magnetic thrust T_B (green triangles) seems to have a limitation: with configuration SM at 0.7 sccm, T_B has a maximum value around 355 µN at 43 W, and further increase of power at 55 W results in a decrease of T_B to 330 µN. It is noteworthy that similar maximum T_B values (around 350 µN and 500 µN) are obtained with configurations SM and BM at 0.7 sccm and 1 sccm.

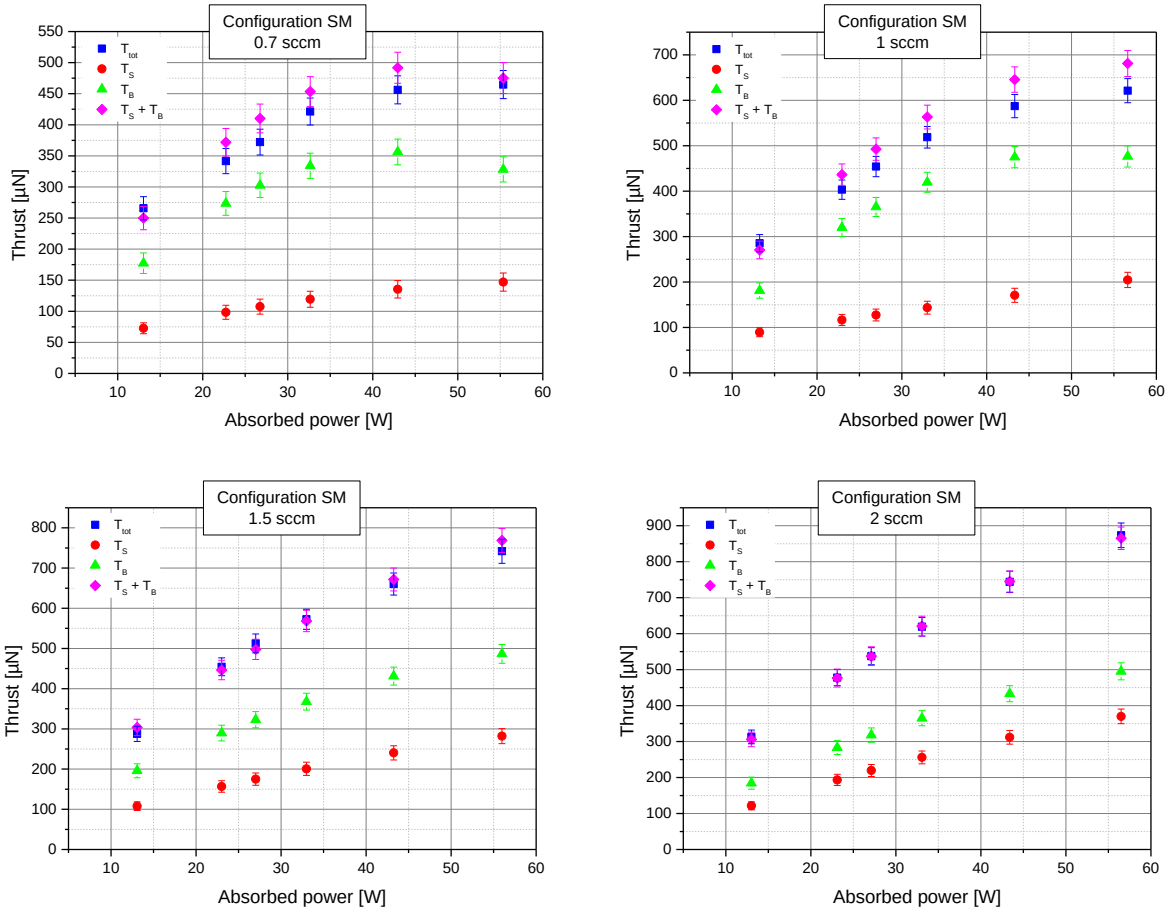

Figure 4. Total thrust T_{tot}, magnetic thrust component T_B, and thermal thrust component T_S vs absorbed power for different xenon flowrates with magnetic configuration SM.

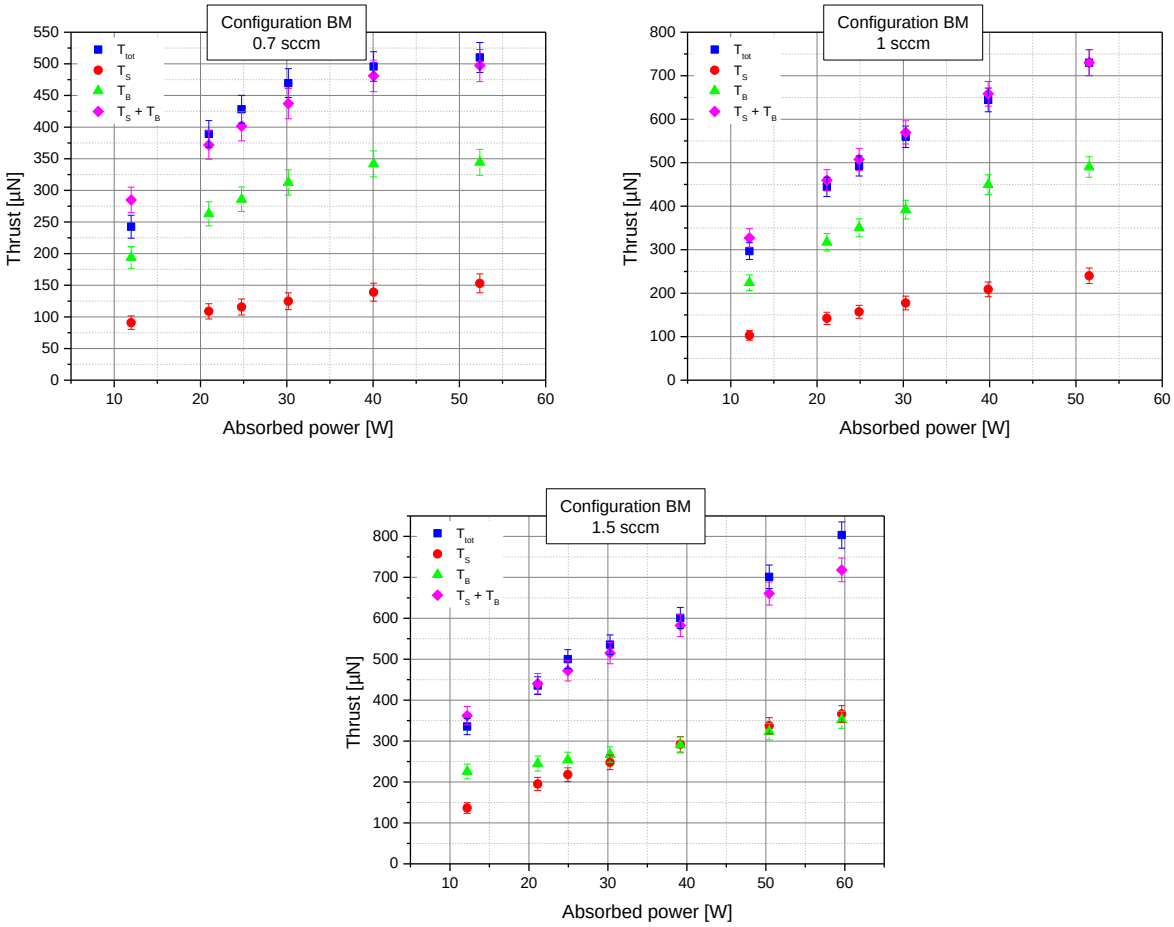

Figure 5. Total thrust T_{tot}, magnetic thrust component T_B, and thermal thrust component T_S vs absorbed power for different xenon flowrates with magnetic configuration BM.

The saturation of magnetic thrust, which probably corresponds to higher power losses in the source, leads to a decrease of thrust efficiency, as shown in Figure 6. The best thrust efficiency (5.5%) is obtained with the most divergent magnetic field configuration (BM), at low flowrate (0.7 sccm) and a microwave power of 25 W. Several operating conditions (at 0.7 sccm and 1 sccm) yield efficiency values higher than 5% for BM configuration, while the best efficiency is around 4% with configuration SM. For higher flowrates (1.5 and 2 sccm), the maximum of the thrust efficiency is probably reached beyond the tested range of power. These performances are slightly lower than previous results obtained in the larger diameter vacuum chamber [4]. The background pressure being similar in both chambers, the discrepancy is probably due to facility effects: the thruster is placed closer to grounded structure (i.e. balance parts) than in previous experimental setups. The influence of background pressure and facility effects on ECR thruster performance is discussed in [10]. In optimum testing conditions, the thrust efficiency is seen to significantly increase.

The contribution of magnetic thrust component to total thrust is shown in Figure 7. For a given flowrate, the fraction of magnetic thrust is globally higher with SM configuration (up to 80%) than with BM configuration (maximum around 70%) despite the higher magnetic field divergence of BM. Generally, the contribution of T_B decreases when increasing the mass flowrate. This could be explained by electron-neutral collisions: as the propellant flowrate is increased, the neutral density in the source is increased, which results in a higher collision rate, and hence a conversion of electron gyrokinetic energy into longitudinal energy and electron pressure.

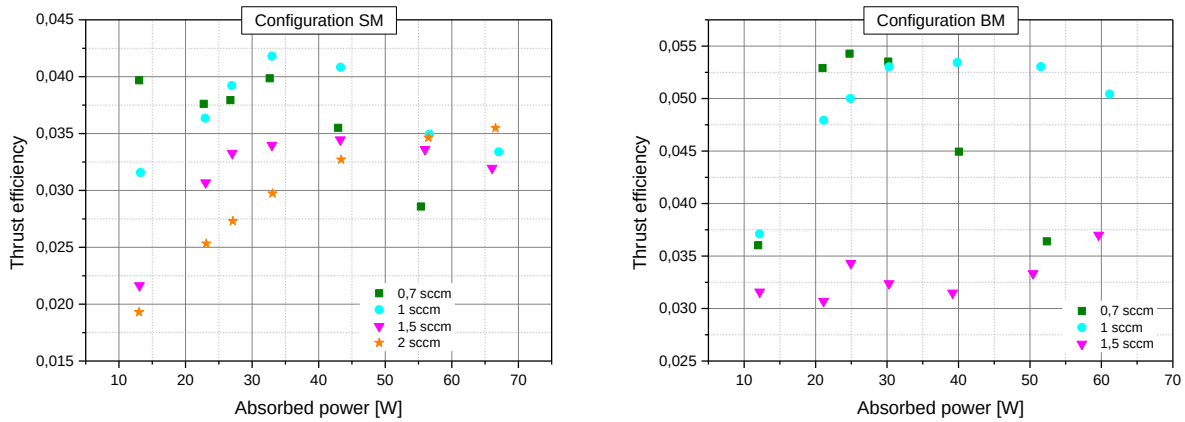

Figure 6. Thrust efficiency vs absorbed microwave power for the magnetic configurations SM and BM.

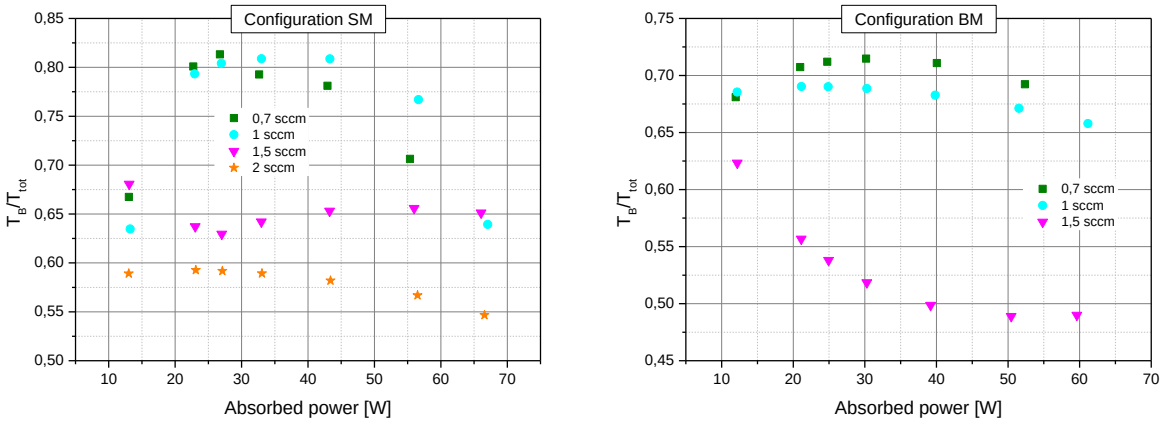

Figure 7. Percentage of magnetic thrust vs absorbed power for different xenon flowrates with magnetic configurations SM and BM.

Even though the electron properties cannot be derived from direct thrust measurements, the comparison of magnetic thrust and thermal thrust can give a first insight on the electron energy anisotropy in the ECR source. Using the fluid model approach, the two thrust components can be expressed as:

$$T_B = \int_z \int_r \mu(r,z) n_e(r,z) 2\pi r \frac{\partial B_z}{\partial z} dr dz \quad (1)$$

$$T_s = \int_r r\, p_{e0,\parallel}(r) dr \quad (2)$$

where μ is the mean value of the magnetic moment of electrons, n_e is the electron density, $p_{e0,\parallel}$ is the electron pressure parallel to thrust axis.

$$\mu = \frac{E_{e,\perp}}{B} \quad (3)$$

μ is an adiabatic invariant.

Under the assumption of uniform radial distribution of electron density in the source, thermal thrust can be expressed as:

$$T_s = p_{e0,\parallel} A_S \quad (4)$$

where A_S is the cross section of the coaxial cavity.

As the electron density is high in the source and dramatically drops in the expansion region, one can assume that T_B is mainly produced in the source. Further analyses that combine thrust measurements with electron density maps have actually shown that the magnetic thrust produced in the source $T_{B,source}$ represents around 75% of T_B [9]. Magnetic thrust can then be approximated:

$$T_B = \langle \mu_s \rangle \langle n_{eS} \rangle \int_z \int_r 2\pi r \frac{\partial B_z}{\partial z} dr dz \quad (5)$$

where $\langle \mu_s \rangle$ is the equivalent average magnetic moment of electrons in the source, and $\langle n_{eS} \rangle$ is the equivalent average electron density in the source (assuming a uniform density in the source).
The ratio of magnetic thrust to thermal thrust can then be written

$$\frac{T_B}{T_S} = \frac{p_{e,\perp}}{p_{e,\parallel}} \frac{\int_z \int_r 2\pi r \frac{\partial B_z}{\partial z} dr dz}{B A_S} \quad (6)$$

The integral term in equations (5) and (6) is a characteristic of the applied magnetic field, which is computed for both magnetic configurations. Using this approach, the ratio of mean electron perpendicular pressure to mean electron parallel pressure is computed for all thrust measurements. The results are shown in Figure 8 (with electron perpendicular pressure calculated for a magnetic field of 875 Gauss). For both configurations, on the whole range of microwave power, the ratio $\frac{p_{e,\perp}}{p_{e,\parallel}}$ decreases when increasing mass flowrate. This is consistent with the increase of the collision rate, which tends to equalize electron gyrokinetic and longitudinal temperatures.
The dependency of $\frac{p_{e,\perp}}{p_{e,\parallel}}$ on microwave power is more difficult to interpret. For configuration SM, the ratio is almost constant with power at 1.5 and 2 sccm, whereas the curve is bell-shaped at lower flowrates, with a ratio varying between 3 and 5 at 0.7 sccm. For configuration BM, at 2 sccm, the ratio drops from 2.4 (at 12 W) to 1.4 (at 60 W), which probably reveals the limits of such an approach. A more accurate method that takes into account spatial variations of electron density in the magnetic nozzle and the contribution of the whole plume to the thrust (not only the source region) has been developed in parallel to this work [9]. The values of $\frac{p_{e,\perp}}{p_{e,\parallel}}$ obtained with the latter method at 32 W are plotted with hollow symbols.

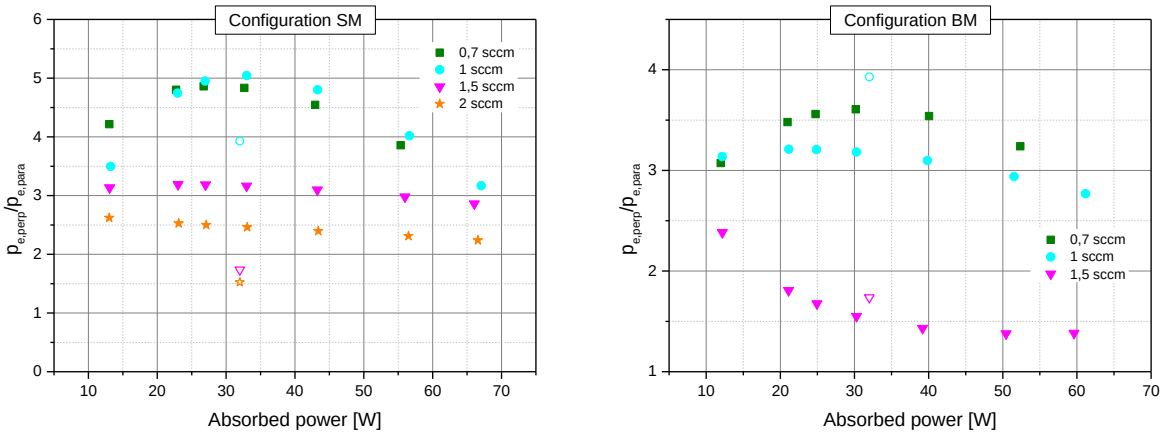

Figure 8. Ratio of mean electron perpendicular pressure $p_{e\perp}$ to mean electron parallel pressurey $p_{e\parallel}$ for the different operating conditions with configurations SM and BM.

IV. Conclusion

Direct thrust measurements of total thrust, magnetic thrust and thermal thrust have been performed on an ECR plasma thruster for various operating conditions, and for two different magnetic field configurations. The typical bell shape of thruster efficiency is well correlated with the saturation of magnetic field.

The contribution of magnetic thrust to total thrust can be as high as 80%, and decreases when increasing mass flow rate. Counter-intuitively, the magnetic field contribution is generally higher for the magnetic field configuration with the lowest divergence.

A further analysis of the electron properties (which is the subject of another paper [9]) can be made by combining these thrust component measurements with electron density maps and magnetic field maps of the plume.

References

[1] Fruchtman, A., Takahashi, K., Charles, C., and Boswell, R. W., "A magnetic nozzle calculation of the force on a plasma," *Physics of Plasmas*, Vol. 19, 033507, 2012.

[2] Takahashi, K., Lafleur, T., Charles, C., Alexander, P., and Boswell, R. W., "Electro diamagnetic effect on axial force in an expanding plasma: Experiments and theory," *Physical Review Letters*, Vol. 107, 235001, 2011.

[3] Takahashi, K., Charles, C., and Boswell, R. W., "Approaching the theoretical limit of diamagnetic-induced momentum in a rapidly diverging magnetic nozzle," *Physical Review Letters*, Vol. 110, 195003, 2013.

[4] Vialis, T., Jarrige, J., Aanesland, A., and Packan, D., "Direct thrust measurements of an electron cyclotron resonance plasma thruster," *Journal of Propulsion and Power*, Vol. 34, No. 5, 2018.

[5] Rafalskyi, D., and Aanesland, A., "A neutralizer-free gridded ion thruster embedded into a 1U cubesat module" *35th Int. Electr. Prop. Conf.*, Atlanta, 2017, IEPC-2017-94

[6] Pavarin, D., Ferri, F., Manente, M., Lucca Fabris, A., Trezzolani, F., Faenza,M., Tasinato, L., Tudisco, O.,Deangelis,R., and Loyan,A., et al., "Thruster Development Set-Up for the Helicon Plasma Hydrazine Combined Micro Research Project (HPH.com)," *35th Int. Electr. Prop. Conf.*, 2011, IEPC-2011-241

[7] Gurciullo, A., Jarrige, J., Lascombes, P., and Packan, D., "Experimental performance and plume characterization of a miniaturized 50W Hall thruster," *36th Int. Electr. Prop. Conf.*, Vienna, 2019, IEPC-2019-142

[8] Jarrige, J., Correyero, S., Elias, P.-Q., and Packan, D., "Investigation on the ion velocity distribution in the magnetic nozzle of an ECR plasma thruster using LIF measurements," *35th Int. Electr. Prop. Conf.*, Atlanta, 2017, IEPC-2017-382

[9] Boni, F., Désangles, V., and Jarrige, J., "Plasma expansion and electron properties in an electron cyclotron resonance plasma thruster," *37th Int. Electr. Prop. Conf.*, Boston, 2022, IEPC-2022-527.

[10] Désangles, V., Packan, D., Jarrige, J., Peterschmitt, S., Dietz, P., Scharmann, S., Holste, K., and Klar, P., "ECRA thruster advances, 30W and 200W prototypes latest performances," *37th Int. Electr. Prop. Conf.*, Boston, 2022, IEPC-2022-513.